

Two Charging Mechanisms in Contact Electrification of Liquid and Ice

Rutvik Lathia¹; Benjamin Leibauer¹; Aaron D. Ratschow¹; Werner Steffen¹ and Hans-Jürgen Butt^{1,*}

¹ Max Planck Institute for Polymer Research, Ackermannweg 10, 55128 Mainz, Germany

*Corresponding author: butt@mpip-mainz.mpg.de

Abstract

The microscopic and fundamental origin of slide electrification, where droplets of water move across insulating surfaces accumulating and depositing electrical charges, is still debated. Charge transfer is often attributed to ion transfer at the receding contact line. However, it is still unclear whether ion transfer alone can fully account for the observed charge separation. We examined slide electrification of two polar, self-ionizing liquids (water, formamide) and two non-polar liquids (diiodomethane, bromonaphthalene). By cooling below the melting temperature, we were able to compare this process to tribocharging of the respective frozen components. Despite having ions immobilized at sub-freezing temperatures, the ice of the polar liquids continues to accumulate significant charge. Non-polar liquids exhibit lower charging (<25% of polar liquids) and nearly identical charging behaviour in both their liquid and frozen phases on five different substrates. Since non-polar liquids contain few free ions, these observations indicate an alternative charging mechanism, which could be electron transfer. Our findings suggest that slide electrification operates through two mechanisms, with the dominant charge transfer pathway shifting between ions and electron transfer depending on the electronegativity, phase, and temperature.

Keywords

Slide electrification; ion and electron transfer; ice electrification; polar and non-polar liquid charging

Water droplets sliding over insulating and hydrophobic surfaces can accumulate electric charge. Consequently, the solid surfaces underneath a droplet acquire opposite charges, a process referred to as slide^{1,2} or contact electrification, analogous to triboelectricity between solids.³ While the charging of droplets is recognized for over a century,^{4,5} quantitative experiments have been scarce until recent times. Only in the past decade methods have emerged to quantify this charging process.⁶⁻⁹ Understanding the mechanisms behind water droplet electrification is essential to understanding dynamic wetting and holds significant implications in many areas related to condensation, energy generation, printing, and desalination.¹⁰⁻¹²

Despite extensive efforts, the microscopic origin of charge transfer in slide electrification remains debated.¹³⁻¹⁵ For liquid water, the prevailing view attributes charging primarily to surface charges, which form spontaneously at the water-solid interface. Usually, the bound surface charges are formed by dissociation of surface groups such as amino groups¹⁶ or the adsorption of ions that remain on the solid surface at the receding contact line. The counterions in the electric double layer accumulate in the sliding drop.^{2,17,18} For hydrophobic surfaces there is still no consensus of how surface charges are formed.^{13-16,19} Zeta potential measurements,²⁰ potentiometric titration^{21,22} and surface force experiments²³ demonstrate that they are usually negatively charged and suggest that in this case an enrichment of OH⁻ at the interfaces leads to surface charging. As an alternative to ion transfer, an electron transfer has been proposed as an additional mechanism, wherein direct electronic exchange due to electron cloud overlap of the solid–liquid interface contributes to surface charging.^{13-15,19}

It is well known that ice-vapor and ice-solid interfaces of water are usually charged.²⁴⁻²⁷ Tribocharging of solid surfaces by ice can lead to charge densities above 1 mC/m². The effect has even been utilized to build triboelectric nanogenerators.^{28,29} For ice, the formation of the diffuse part of an electric double layer will be suppressed. Although it is well-established that a liquid-like layer exists on the surface of ice and at the solid-ice interface, this layer is much thinner than the electric double layer. Furthermore, its thickness decreases with decrease temperature to below 1 nm.³⁰⁻³²

Here, to elucidate the fundamental process(es) of charge transfer, we studied the tribocharging and the slide electrification of frozen and liquid water, formamide (both polar), diiodomethane and 1-bromonaphthalene (both non-polar). To gain further insight, we performed the experiments on five

chemically different surfaces. Using a tilted plate setup with capacitive current detection⁹, we quantified charge accumulation under controlled temperature conditions. Our results showed that the frozen state of polar liquids, despite having immobilized ions, continued to charge significantly, with enhanced charging near the melting transition. Nonpolar liquids, in both liquid and frozen phases, displayed consistent charge deposition indicating an additional mechanism.

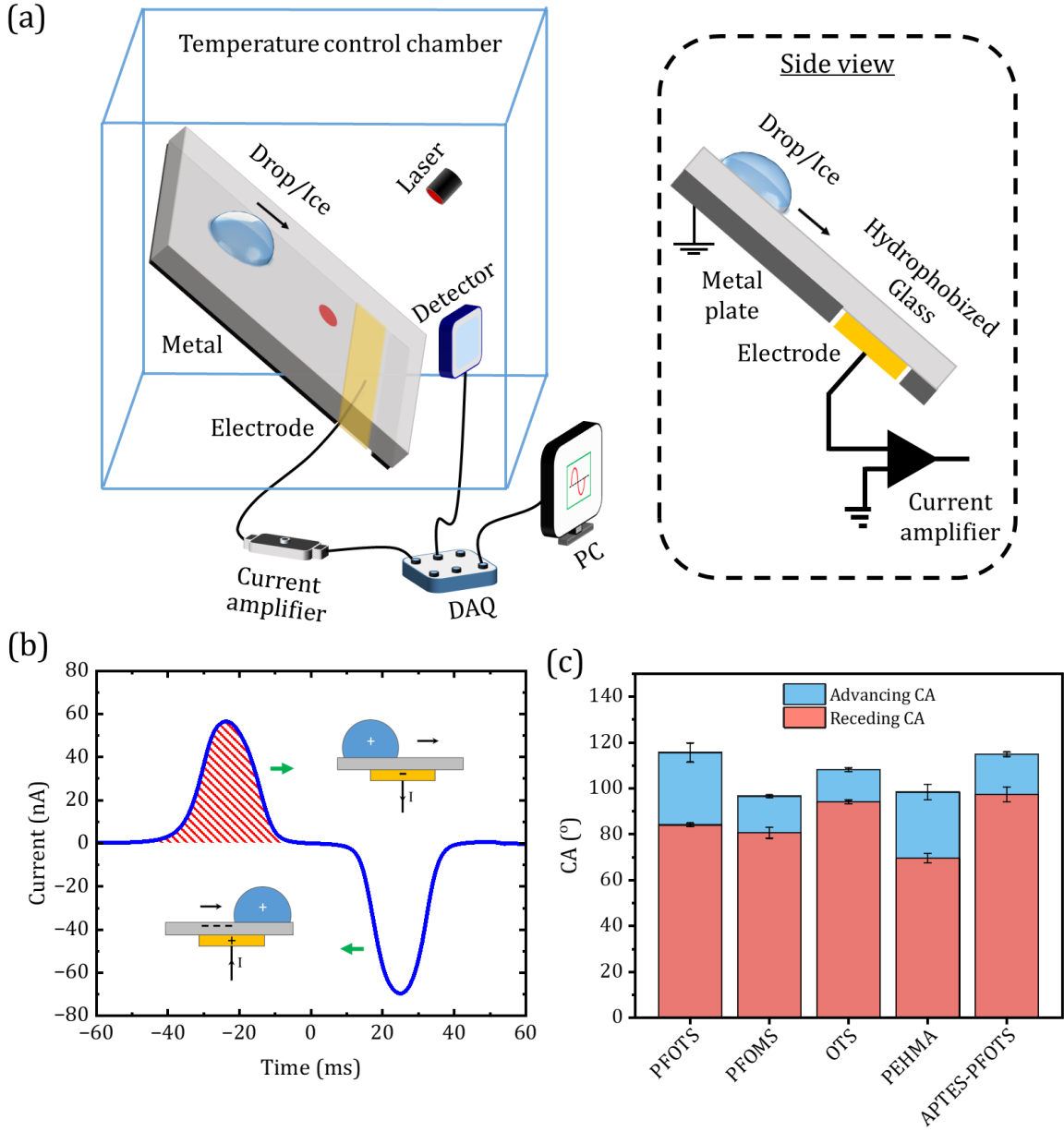


Fig. 1: (a) Setup for measuring the charge on droplets and ice. The setup consists of a hydrophobized glass plate inclined by 50° with a copper electrode at its back connected to a current amplifier for signal detection. A laser and detector were placed 10 mm above the bottom electrode (red dot) to trigger the recording of the signal. The current signal was amplified and

recorded by data acquisition (DAQ) system. (b) The recorded signal from a 50 μL water droplet sliding on OTS coated glass. The first peak corresponds to the accumulated charge in a droplet while the second (inverse peak) represents the deposited charge due to slide electrification in addition to charge on a drop. The red shaded area was integrated to determine the accumulated charge on the droplet. (c) Advancing and receding contact angles of water drops on various hydrophobic coatings on glass. Error bar represents standard deviation of 3 measurements.

To measure the charge deposited by the liquid/solid phase we used a tilted plate setup enclosed in a temperature controlled chamber ([Fig. 1a](#)).⁹ Drops/ice slide down a hydrophobized glass plate. A copper electrode of 20 mm length at the back of the substrate was connected to a current amplifier to detect the drop charge. It was positioned at a drop/ice sliding distance of 40 mm.² While a droplet slides down the solid surface it acquires an electrical charge and leaves an opposite charge on the surface. The sliding distance (40 mm) was chosen such that drop/ice is saturated with charge.³³ We measured the resulting capacitive current induced when the charged drop slides over the electrode. When a charged drop passes over the electrode, it generates a bipolar induced current signal ([Fig. 1b](#)) due to the generation of image charges. For a water droplet sliding over octyltrichlorosilane (OTS) coated glass, the first peak is a positive current peak due to the accumulated positive droplet charge. Electrons are flowing into the electrode. After the drop passes the center of the electrode, the current reverses to a negative peak due to electrons flowing back to ground. We integrate the first half of the bipolar current peak to estimate the amount of accumulated charge (red shaded area in [Fig. 1b](#)). The surface is initially neutralized with an ion gun thus the recorded drop charges correspond to the charges of the first drop sliding on a previously uncharged surface. Advancing and receding contact angles of water drops on various hydrophobic coating are given in [Fig. 1c](#). Characterization and properties of surfaces and liquids used are given in [Supplementary Fig. S1 & S2](#) and [Table 1](#).

As an example, we present the drop charges measured using OTS-coated glass, as these surfaces lead to strong charge separation ([Fig. 2](#)). Within a temperature range of 0 to 20°C, a 50 μL water drop accumulates a charge of around 1 nC. Following the common theory, we attribute this signal to adsorbed hydroxide ions (OH^-).^{1,2,18,34,35} Water contains hydroxide ions and hydronium ions (H_3O^+) due to self-ionization. During its interaction with the hydrophobic surface, OH^- ions are adsorbed at the surface-liquid interface and form the electrical double layer (EDL).²⁰ Upon dewetting, some OH^- ions stay on the surface, resulting in a negatively charged surface. The water

droplets accumulate H_3O^+ ions, resulting in net positive charge. We would like to point out that it has not yet been proven that hydroxide ions cause slide electrification, and that other ions (e.g. carbonate) may also be involved.³⁶

Table 1: Properties of liquids used in the study at 20°C.

Property	Water	Formamide	Diiodomethane	1-Bromonaphthalene
Surface tension (mN/m)	72	58	51	44
Dielectric constant (ϵ_r)	80	111	5.3	4.8
Melting point (°C)	0	2	6	-2
Density (g/cm³)	0.997	1.13	3.306	1.48
Viscosity (mPa·s)	0.89	3.3	2.6	4

Ice showed lower and a constant charge (~ 0.6 nC) at temperatures $\leq -5^\circ\text{C}$. Near the melting point, the charge (Fig. 2) was even higher with ice (~ 2.1 nC) than with a water droplet (~ 1.2 nC). The pronounced increase in deposition rates near 0° C cannot be explained solely by this ionic transfer mechanism, suggesting that additional processes become dominant in this regime.³⁰ Similar charging behaviour – high charging for the liquid, low charging for ice at or below 5° C and a peak near the melting point - was observed for perfluoroctyltrichlorosilane (PFOTS) and chloro(dimethyltridecafluoroctyl)silane (PFOMS) coated substrates (Fig. 3).

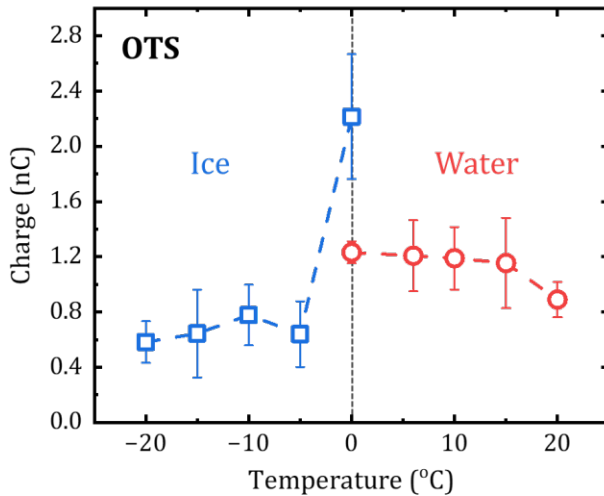


Fig. 2: Charge of water drops (red) and ice (blue) created on OTS coated glass upon varying the temperature.

The two charging regimes for ice and water and the peak in between indicate that two different charge transfer processes prevail. For water at $T \geq 0^\circ\text{C}$ the results agree with the deposition of anions from the electric double layer. Below 0°C , for ice, the formation of a diffuse layer is hindered. It is established that a liquid-like layer exists at the ice–vapor and at ice–solid interfaces.³⁷ This quasi-liquid layer, which forms due to surface premelting,³⁰⁻³² can enable OH^- ion transfer and deposition onto the surface. The thickness of this layer is highly temperature dependent.³⁸ Below approximately -16°C it is reduced to the order of a bilayer of water molecules.³⁸ This layer is much thinner than the typical Debye length of an aqueous electric double layer (~ 100 nm). Moreover, our measurements show no temperature dependence of charge deposition that would correlate with changes in liquid-like layer thickness. However, protons and hydroxides still exist which can diffuse and cause significant charging. In addition, formamide, another polar self-ionizing liquid ($2\text{HCONH}_2 \rightleftharpoons \text{HCONH}_3^+ + \text{HCONH}_3^-$, $\text{pK}_a = 16.8$),³⁹ showed charging behaviour analogous to that of water (Supplementary Fig. S3).

A possible second mechanism, which may dominate below 0°C involves electron (e^-) transfer driven by direct contact between the ice and the substrate during sliding.⁴⁰ In this scenario, the overlap of electron clouds at the interface facilitates net electron transfer from the ice to the surface,

leading to negative surface charging. However, there is no direct evidence of e^- transfer. Near 0°C, the simultaneous presence of both solid and liquid water phases can promote a hybrid charging mechanism, where electron transfer coexists with ionic (OH^-) transfer, enhancing the overall deposition rate and thus, increasing the charge on ice.³⁰ Moreover, in water, stable formation of EDL may hinder these additional charge carriers due to an additional potential barrier.

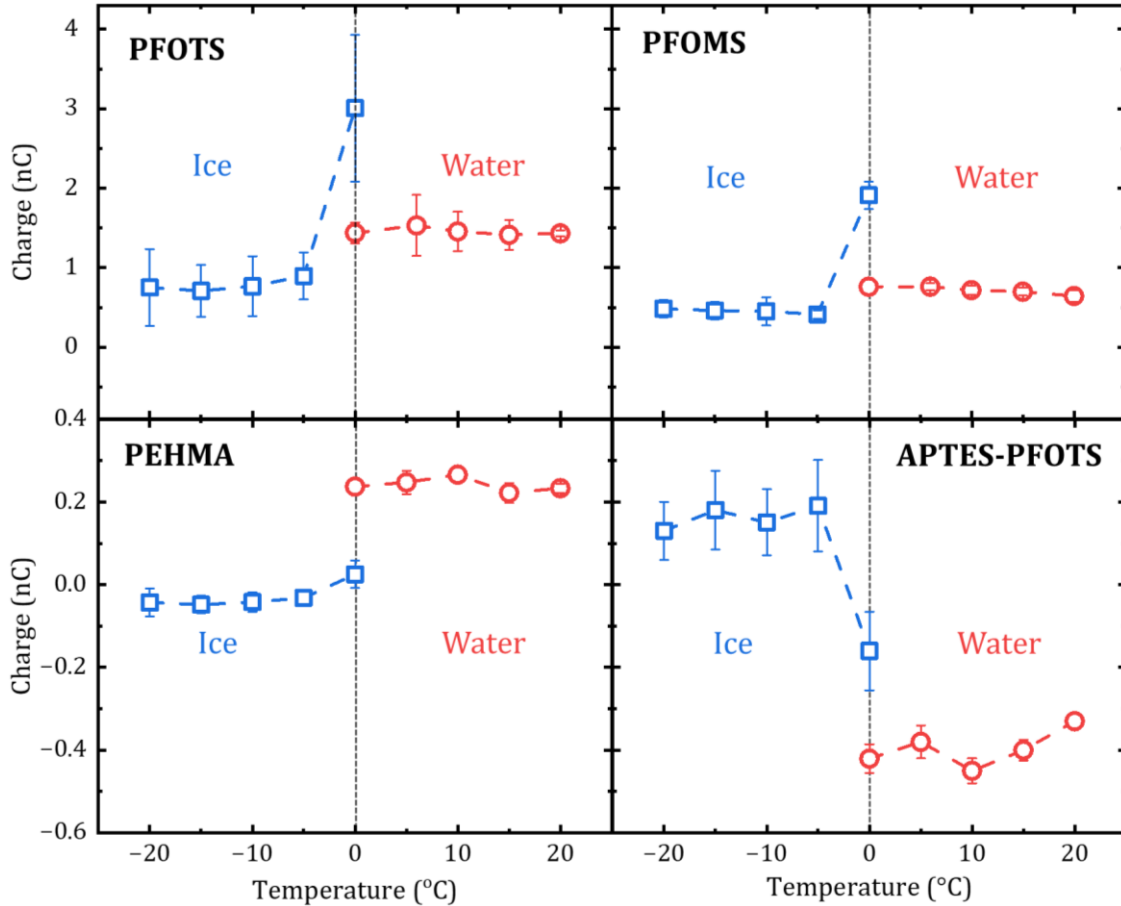


Fig. 3: Drop charge versus temperature measured on a PFOTS, PFOMS, PEHMA and APTES-PFOTS coated glass.

Ice and water do not always charge in the same polarity (Fig. 3). For poly(2-ethylhexyl methacrylate) (PEHMA)-coated glass, interaction with a water droplet results in a positive charge of +0.25 nC, which is consistent with OH^- adsorption from the liquid onto the surface (Fig. 3). In contrast, when the same coating interacts with ice at temperatures at or below -5°C , a net negative

charge of -0.05 nC is accumulated (Fig. 3). This polarity switch cannot be explained by ions alone, pointing towards an alternate mechanism. The effect is reversed for (3-aminopropyl)-triethoxysilane (APTES)-PFOTS coatings, where water charges negatively and ice positively (Fig. 3). The amine group gets protonated from the sliding water drop ($\text{R-NH}_2 + \text{H}^+ \rightarrow \text{R-NH}_3^+$), resulting in a net positive surface charge when contacted by water at near-neutral pH; the surface pK_a of primary APTES layers is ~ 9.6 so a significant fraction is protonated under our conditions.^{16,41} As a result, the drop charges negatively. However, ice may transfer e^- to the surface, making it negatively charged. At 0°C , the measured charge for both coatings lies between that water and ice values. This is consistent with a regime where ion and electron transfer occur simultaneously but in opposite directions, partially cancelling one another and yielding a reduced net charge. The polarity inversion suggests that ion transfer from the quasi-liquid layer does not fully account for ice charging below -5°C .

To find out whether ion-based charge separation is necessary for slide electrification, we carried out charge measurements with nonpolar liquids which still have a high surface tension, such as diiodomethane and 1-bromonaphthalene. In contrast to the polar liquids tested, the number of free ions and the formation of an EDL should be negligible.⁴² Moreover, our tested polar liquids are self-ionizing in nature while non-polar liquids are not. Drop charging was reduced to 30-50% compared to that of water (Fig. 4). For the non-polar liquids, drop charging decreased to $\leq 25\%$ and even charge reversal was observed for OTS and PEHMA coated surfaces. Significant charge with nonpolar liquids suggests a presence of an alternate mechanism (Fig. 4). Because nonpolar liquids have a relatively low dielectric constant ($\epsilon_r = 5.3$ for diiodomethane and 4.8 for 1-bromonaphthalene) as compared to polar liquids ($\epsilon_r = 80$ for water and 111 for formamide), the electrostatic energy cost of separating charges is high ($U \sim 1/\epsilon_r$). The much larger U in nonpolar liquids implies that ion pairs are much more tightly bound and spontaneous ion separation is strongly suppressed.⁴² Thus, higher energy cost suppresses ion-based charge separation during sliding. However, other charging pathways (i.e., electrons) can still operate and result in significant deposition.

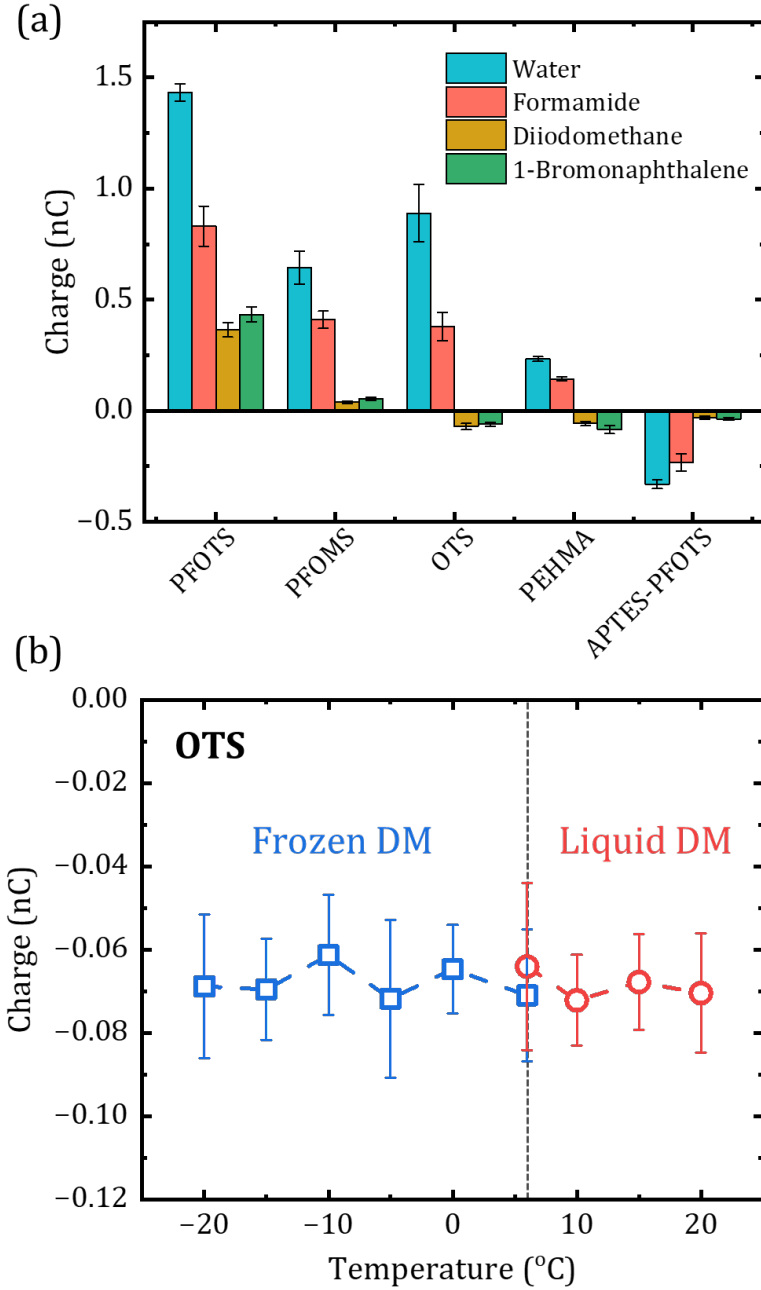


Fig. 4: (a) A comparison of charge on polar (water and formamide) and nonpolar (diiodomethane and 1-bromonaphthalene) drops at 20°C on various surfaces. (b) Charge on liquid and frozen phase diiodomethane on OTS coated glass showed consistent behavior without any peak at melting point (6°C, black dotted line).

In Fig. 4a, we compare drop charges measured with different liquids on surfaces with different chemical functionalities. On PFOTS, PFOMS and APTES-PFOTS coatings, all liquids

consistently deposited charges of the same polarity, although the magnitudes differ. Conversely, for OTS and PEHMA coatings, a polarity reversal was observed when switching from polar to nonpolar liquid (Fig. 4a). These results demonstrate that hydroxyl groups (for PFOTS and PFOMS) or protons (APTES-PFOTS) are not the only charges, which are transferred, because they cannot explain the drop charges in diiodomethane and bromonaphthalene.

Furthermore, if water contamination was responsible for the charging by diiodomethane and bromonaphthalene, the polarity would remain consistent with water droplets across all surfaces. We further performed Karl Fischer Coulometry to quantify residual water and found <0.05% water in the nonpolar liquids and <0.4% in formamide. The reversal therefore supports an additional mechanism at play in nonpolar liquids.

We further compare charge deposition with a nonpolar liquid and its frozen phase (Fig. 4b). A liquid diiodomethane droplet (50 μ L) at room temperature accumulated a charge of around -0.07 nC on OTS coated glass. It was independent of temperature for the tested range of -20°C to 20°C . No significant change was detected at the melting point of 6°C between liquid and frozen diiodomethane, which is different from our observation with polar liquids (Fig. 2a). Similar charging behavior was also observed for other hydrophobic substrates and nonpolar liquids (Supplementary Fig. S4 & S5). The observations further indicate that another charging mechanism is dominating. It is consistent with the electron transfer hypothesis: as ions most likely do not contribute to charge deposition in nonpolar liquids, electrons may provide the dominant transfer pathway.

To further analyze a possible contribution of electron transfer to charging, we plotted the average electronegativity of the liquids and the surface functional groups with the polarity of charge deposition. For the nonpolar liquids we found a correlation between the average electronegativity of liquid and the surface functional groups with the polarity of charge deposition. Specifically, the direction of charge transfer is correlated with the difference in electronegativity between the surface coating and the liquid molecules (Fig. 5). Here, the electronegativity difference is defined as $\Delta_{en} = \chi_s - \chi_l$, where χ_s and χ_l are the average Pauling's electronegativities for surface group and liquid molecule, respectively. χ_s and χ_l were calculated by taking arithmetic average of individual atoms' electronegativity.^{43,44} Values are given in Supplementary Table S1. When the average electronegativity of the surface exceeds that of the liquid ($\Delta_{en} > 0$), electrons

preferentially transfer from the sliding liquid to the surface, resulting in a net positive charge of the drop. Conversely, when the liquid has a higher electronegativity ($\Delta_{en} < 0$), electrons transfer from the surface to the liquid, leaving the droplet negatively charged. This correlation provides a straightforward explanation for the polarity reversals observed in [Fig. 4a](#). For example, PFOTS and PFOMS surfaces, which possess more electron-withdrawing groups than the tested nonpolar liquids, can charge liquid positively due to electron donation from the liquid. In contrast, coatings such as OTS and PEHMA, with lower effective electronegativity relative to the liquid, charges liquid negatively.

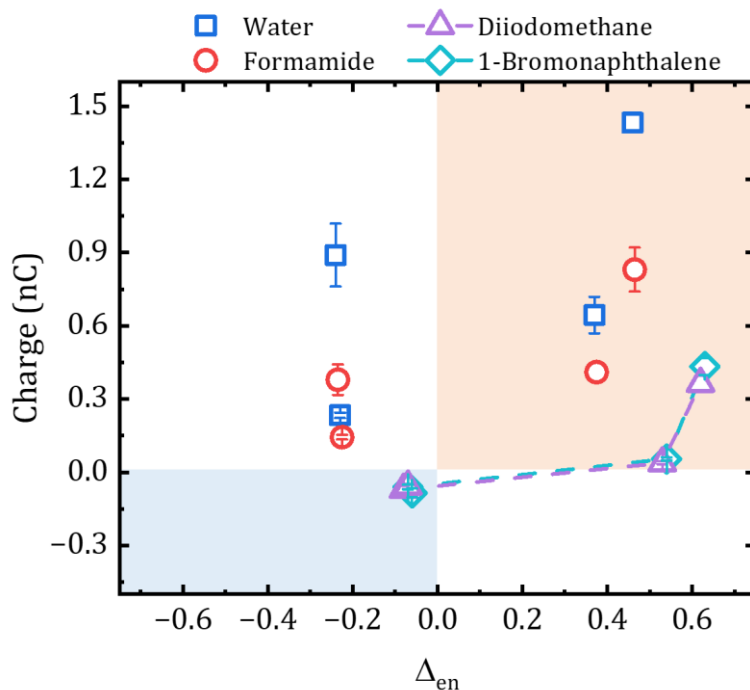


Figure 5: liquid charge variation (20°C) variation with electronegativity difference (Δ_{en}) for polar and nonpolar liquids. The red shaded area represents where droplet charge and Δ_{en} are positive while the blue area represents negative values.

However, polar liquids do not follow this trend, likely due to the dominant contribution from ion transfer. Additionally, no direct correlation was observed between the amount of charge deposition and Δ_{en} , as charge deposition is influenced by multiple factors, including surface wettability, droplet velocity, sample preparation, and surface roughness. Furthermore, the electronegativity of the outermost exposed surface groups is likely to play a more significant role in the charge transfer process than that of the inner functional groups. These results suggest that interfacial electron

transfer is governed by relative electronegativity differences, and provide a predictive descriptor for charge polarity in liquid–solid triboelectrification. While our observations strongly indicate a contribution from electron transfer as an additional mechanism, direct evidence for electron involvement remains lacking.

Conclusion

Our study indicates that slide electrification is governed by a combination of two fundamental charge transfer mechanisms, with their relative contributions determined by the liquid’s polarity, ionization, phase, temperature, and the electronegativity difference between liquid and surface. Polar liquids primarily transfer ions in their liquid state, whereas an additional mechanism dominates in frozen states and in nonpolar liquids. Near the melting point of polar liquids, both mechanisms can operate simultaneously, resulting in enhanced or intermediate charge deposition depending on the surface and liquid properties. These findings establish a unified framework for understanding charge generation in liquid–solid interactions and highlight the fundamental role of an additional mechanism alongside ions in governing surface charging across diverse materials and conditions.

Methods

Experimental details:

All measurements were carried out on a tilted plate setup inside a temperature-controlled chamber. The temperature of the chamber was maintained within a resolution of $\pm 1^\circ\text{C}$. Four different liquids were used: deionized water (Milli-Q, 18.2 M Ω .cm), formamide (99.5%, AppliChem GmbH), diiodomethane (>99%, Thermo Scientific) and 1-bromonaphthalene (>95%, Sigma Aldrich). A 50 μL droplet was frozen on a hydrophobized silicon wafer to ensure a smooth, flat interface ([Supplementary Fig. S6](#)). The frozen droplet was carefully removed from the silicon wafer with a metal tweezer. The same hydrophobic coating on glass was used for charge measurement to avoid cross-contamination. For charge measurements, liquid droplet/ice (50 μL) was dispensed on a

hydrophobic glass surface on a tilted plate (50°). A copper electrode of $20 \times 25 \text{ mm}^2$ area and 3 mm thickness was placed on the backside of the surface at the sliding distance of 40 mm. The size of the electrode is significantly larger than used in the literature.⁹ The electrode needs to be much larger than the drop size to avoid an overlapping of the bi-polar peaks. If the two peaks overlap, they partly cancel each other out, which leads to an underestimation of the charge value. It is necessary to ensure two completely separated peaks for correct charge determination as shown in [Fig. 1b](#). The remaining part of the glass plate was placed on a grounded metal plate. The electrode was connected to a current amplifier (DDPCA-300, FEMTO) and data acquisition system - DAQ (USB-6366, NI) to record the current signal. Amplification used was in the range of 10^7 to 10^9 V/A depending upon the sample with rise times of 0.8 ms to 2.3 ms. A light barrier formed by a laser and a detector (placed 10 mm above the electrode) was employed to detect the incoming droplet/ice to trigger the recording of the current signal. All components of the setup were kept at the same temperature, except the amplifier and DAQ. All the surfaces were neutralized by Zerostat anti-static ion gun (Sigma Aldrich) before the experiments to neutralize the surface from any residual charge. Liquid droplets and ice were handled with grounded metal syringe and metal tweezer, respectively to avoid any pre-charging. Each experiment involved at least 5 measurements on different surfaces, which were utilized to calculate of the standard deviation. Additionally, surface was neutralized with ion gun before each measurement.

Preparation of surfaces:

Glass slides ($76 \times 26 \times 1 \text{ mm}^3$, soda-lime, epredia) were used as a substrate for various hydrophobic coating. The protocol for preparation is available in literature.^{9,16} Glass slides were first cleaned with ethanol and isopropyl alcohol under 10 min of ultra-sonication and blow-dried with nitrogen. O₂ plasma (Diener electronic, with 300 W and 0.3 bar for 10 minutes) was used to activate the surface before coating. Activated glass slides were placed inside a vacuum desiccator with 1 mL vial of 1H,1H,2H,2H-perfluorooctyltrichlorosilane (PFOTS, 97%, TCI) solution. The desiccator was evacuated with a vacuum pump to less than 50 mbar for 10 min – allowing PFOTS vapor to fill the entire chamber. Then the reaction was allowed to take place for 20 minutes at constant pressure after closing the chamber. The PFOTS-coated slides were rinsed with ethanol multiple times to rinse off unreacted silane⁴⁵ and dried with nitrogen before using them for charge

measurements. The same process was followed for octyltrichlorosilane (OTS, 97%, Sigma-Aldrich) and chloro(dimethyltridecafluoroctyl)silane (PFOMS, >94%, TCI) coating. Additionally, we prepared mixed PFOTS-APTES-coated glass.¹⁶ In this case, we started with a PFOTS primary coating with a reaction time of 10 min. Then (3-aminopropyl)triethoxysilane (APTES, 99%, Sigma-Aldrich) secondary coating was deposited in separate desiccator with 6 h of reaction time at 50 mbar chamber pressure.

We synthesized the grafted poly(2-ethylhexyl methacrylate) (PEHMA) surfaces in the same way as described previously.⁴⁶ Copper(I) bromide (>98%, TCI) was purified before the synthesis.⁴⁷ All other chemicals were used as delivered. 2-Ethyl methacrylate (EHMA, 7.04g, 35.51 mmol, Sigma Aldrich), 4,4'-dinonyl-2,2'-dipyridyl (58.6 mg, 0.143 mmol, TCI), copper(II) bromide (6.6 mg, 0.029 mmol, Sigma Aldrich) and toluene (>99.8%, Fisher, Netherland)/DMSO (5.3 mL: 2.6 mL, puriss. p.a. dried <0.02%, Sigma Aldrich) were added to a flask, provided with a septum and degassed with argon for 1 h. After degassing, the copper(I) bromide was transferred with a syringe to the degassed (30 minutes) reaction reactors, containing the Br-SAM grafted substrate. The syringe was degassed with argon three times before using. The polymerization was performed at 30°C. After the desired reaction time, the reaction was terminated by rinsing the polymer brush surfaces two times with toluene, ethanol and DI-water once the desired thickness is reached (12 nm).

Characterization:

Contact angle measurements were carried out using a Krüss goniometer to evaluate surface wettability. Advancing and receding contact angles were determined by gradually adding and withdrawing liquid (5 μ L/min) into a droplet of deionized water (5–35 μ L) on the sample surface for 3 cycles (Fig. 1c). Surface topography and roughness were characterized using Atomic Force Microscopy in tapping mode (AFM, Dimension ICON FastScan). [Supplementary Fig. S1](#) represents AFM topography and roughness characterization of all the samples.

The X-ray diffraction (XRD, Rigaku SmartLab, 1.54 \AA wavelength) measurements for the all the frozen samples are given in [Supplementary Fig. S2](#). All the liquids were frozen first on OTS-coated silicon wafers and subsequently transferred to the XRD chamber in liquid nitrogen (Formamide

was frozen directly by liquid nitrogen). During XRD, temperature was kept constant at -20° C for water, diiodomethane and 1-bromonaphthalene while -50° C for formamide. The ice phase of water showed mostly hexagonal structure ([Supplementary Fig. S2](#)).⁴⁸

The Karl Fischer Coulometry was performed with a Mettler Toledo C20 compact coulometer using a 1 mL syringe. 1 mL of the solvent was taken with the syringe. The analyte was weighted and the water content was measured by the Karl Fischer Coulometry. Every solvent was measured at least three times. Water content by volume of solvent found was 0.051 ± 0.001 % in diiodomethane, 0.024 ± 0.003 % in 1-bromonaphthalene and 0.38 ± 0.04 % in formamide.

Author Contributions

H.J.B. and R.L. conceived the project. R.L. designed experiments and carried out charge measurements. B.L. and R.L. prepared and characterized samples. A.D.R. devised the measurement method. H.J.B. and W.S. supervised the project. R.L. wrote the manuscript. H.J.B., W.S., R.L., B.L. and A.D.R. discussed results, reviewed and revised the manuscript.

Acknowledgement

This work was supported by the European Union’s ERC Advanced Grant No. 883631 “DynaMo”. Authors acknowledge Rüdiger Berger for providing the temperature-controlled chamber and Pravash Bista for help in initial setup.

References

- 1 Yatsuzuka, K., Mizuno, Y. & Asano, K. Electrification phenomena of pure water droplets dripping and sliding on a polymer surface. *Journal of Electrostatics* **32**, 157-171 (1994). [https://doi.org/10.1016/0304-3886\(94\)90005-1](https://doi.org/10.1016/0304-3886(94)90005-1)
- 2 Stetten, A. Z., Golovko, D. S., Weber, S. A. & Butt, H.-J. Slide electrification: charging of surfaces by moving water drops. *Soft Matter* **15**, 8667-8679 (2019). <https://doi.org/10.1039/C9SM01348B>

3 Wang, Z. L. From contact electrification to triboelectric nanogenerators. *Reports on Progress in Physics* **84**, 096502 (2021). <https://doi.org/10.1088/1361-6633/ac0a50>

4 Thomson, J. J. XXXI. On the electricity of drops. *The London, Edinburgh, and Dublin Philosophical Magazine and Journal of Science* **37**, 341-358 (1894). <https://doi.org/10.1080/14786449408620555>

5 Nolan, J. Electrification of water by splashing and spraying. *Proceedings of the Royal Society of London. Series A, Containing Papers of a Mathematical and Physical Character* **90**, 531-543 (1914). <https://doi.org/https://doi.org/10.1098/rspa.1914.0081>

6 Li, X., Ratschow, A. D., Hardt, S. & Butt, H.-J. Surface charge deposition by moving drops reduces contact angles. *Physical Review Letters* **131**, 228201 (2023). <https://doi.org/10.1103/PhysRevLett.131.228201>

7 Xu, W. *et al.* Triboelectric wetting for continuous droplet transport. *Science Advances* **8**, eade2085 (2022). <https://doi.org/10.1126/sciadv.ade2085>

8 Bista, P., Ratschow, A. D., Butt, H.-J. r. & Weber, S. A. High voltages in sliding water drops. *The Journal of Physical Chemistry Letters* **14**, 11110–11116 (2023). <https://doi.org/10.1021/acs.jpcllett.3c02864>

9 Bista, P., Ratschow, A. D., Stetten, A. Z., Butt, H.-J. & Weber, S. A. L. Surface charge density and induced currents by self-charging sliding drops. *Soft Matter* **20**, 5045-5052 (2024). <https://doi.org/10.1039/D4SM00205A>

10 Jin, Y. *et al.* Electrification of water: From basics to applications. *Droplet* **1**, 92-109 (2022). <https://doi.org/10.1002/dro2.22>

11 Xu, W. *et al.* A droplet-based electricity generator with high instantaneous power density. *Nature* **578**, 392-396 (2020). <https://doi.org/10.1038/s41586-020-1985-6>

12 Lathia, R. *et al.* Advances in microscale droplet generation and manipulation. *Langmuir* **39**, 2461-2482 (2023). <https://doi.org/10.1021/acs.langmuir.2c02905>

13 Lin, S., Xu, L., Wang, A. C. & Wang, Z. L. Quantifying electron-transfer in liquid-solid contact electrification and the formation of electric double-layer. *Nature communications* **11**, 1-8 (2020). <https://doi.org/10.1038/s41467-019-14278-9>

14 Lin, S., Chen, X. & Wang, Z. L. Contact electrification at the liquid–solid interface. *Chemical Reviews* **122**, 5209-5232 (2021). <https://doi.org/10.1021/acs.chemrev.1c00176>

15 Zhan, F. *et al.* Electron transfer as a liquid droplet contacting a polymer surface. *ACS nano* **14**, 17565-17573 (2020). <https://doi.org/10.1021/acs.nano.0c08332>

16 Wong, W. S. *et al.* Tuning the charge of sliding water drops. *Langmuir* (2022). <https://doi.org/10.1021/acs.langmuir.2c00941>

17 Beattie, J. K. The intrinsic charge on hydrophobic microfluidic substrates. *Lab on a Chip* **6**, 1409-1411 (2006). <https://doi.org/10.1039/B610537H>

18 Ratschow, A. D. *et al.* How charges separate when surfaces are dewetted. *Physical Review Letters* **132**, 224002 (2024). <https://doi.org/10.1103/PhysRevLett.132.224002>

19 Jin, Y. *et al.* How liquids charge the superhydrophobic surfaces. *Nature Communications* **15**, 4762 (2024). <https://doi.org/10.1038/s41467-024-49088-1>

20 Zimmermann, R., Freudenberg, U., Schweiß, R., Küttner, D. & Werner, C. Hydroxide and hydronium ion adsorption — A survey. *Current Opinion in Colloid & Interface Science* **15**, 196-202 (2010). <https://doi.org/https://doi.org/10.1016/j.cocis.2010.01.002>

21 Preočanin, T. *et al.* Surface charge at Teflon/aqueous solution of potassium chloride interfaces. *Colloids and Surfaces A: Physicochemical and Engineering Aspects* **412**, 120-128 (2012). <https://doi.org/https://doi.org/10.1016/j.colsurfa.2012.07.025>

22 Barišić, A. *et al.* Experimental data contributing to the elusive surface charge of inert materials in contact with aqueous media. *Colloids and Interfaces* **5**, 6 (2021). <https://doi.org/https://doi.org/10.3390/colloids5010006>

23 Weidenhammer, P. & Jacobasch, H.-J. Investigation of adhesion properties of polymer materials by atomic force microscopy and zeta potential measurements. *Journal of Colloid and Interface Science* **180**, 232-236 (1996). <https://doi.org/https://doi.org/10.1006/jcis.1996.0294>

24 Petrenko, V. F. & Colbeck, S. C. Generation of electric fields by ice and snow friction. *Journal of Applied Physics* **77**, 4518-4521 (1995). <https://doi.org/10.1063/1.359448>

25 Petrenko, V. F. & Ryzhkin, I. A. Surface states of charge carriers and electrical properties of the surface layer of ice. *The Journal of Physical Chemistry B* **101**, 6285-6289 (1997). <https://doi.org/10.1021/jp963216p>

26 Mukherjee, R., Ahmadi, S. F., Zhang, H., Qiao, R. & Boreyko, J. B. Electrostatic jumping of frost. *ACS Nano* **15**, 4669-4677 (2021). <https://doi.org/10.1021/acsnano.0c09153>

27 Tkachenko, K. & Jacobi, H.-W. Electrical charging of snow and ice in polar regions and the potential impact on atmospheric chemistry. *Environmental Science: Atmospheres* **4**, 144-163 (2024). <https://doi.org/10.1039/D3EA00084B>

28 Ahmed, A. *et al.* All printable snow-based triboelectric nanogenerator. *Nano Energy* **60**, 17-25 (2019). <https://doi.org/https://doi.org/10.1016/j.nanoen.2019.03.032>

29 Luo, N. *et al.* Ice-based triboelectric nanogenerator with low friction and self-healing properties for energy harvesting and ice broken warning. *Nano Energy* **97**, 107144 (2022). <https://doi.org/https://doi.org/10.1016/j.nanoen.2022.107144>

30 Wei, Y. *et al.* Contact electrification at the solid–liquid transition interface. *Materials Today* **74**, 2-11 (2024). <https://doi.org/10.1016/j.mattod.2024.03.013>

31 Li, H. *et al.* Water mobility in the interfacial liquid layer of ice/clay nanocomposites. *Angewandte Chemie International Edition* **60**, 7697-7702 (2021). <https://doi.org/https://doi.org/10.1002/anie.202013125>

32 Rosenberg, R. Why is ice slippery? *Physics Today* **58**, 50-54 (2005). <https://doi.org/10.1063/1.2169444>

33 Ratschow, A. D., Butt, H.-J., Hardt, S. & Weber, S. A. L. Liquid slide electrification: advances and open questions. *Soft Matter* **21**, 1251-1262 (2025). <https://doi.org/10.1039/D4SM01289E>

34 Helseth, L. Electrical energy harvesting from water droplets passing a hydrophobic polymer with a metal film on its back side. *Journal of Electrostatics* **81**, 64-70 (2016). <https://doi.org/https://doi.org/10.1016/j.elstat.2016.03.006>

35 Burgo, T. A. L., Galembeck, F. & Pollack, G. H. Where is water in the triboelectric series? *Journal of Electrostatics* **80**, 30-33 (2016). <https://doi.org/https://doi.org/10.1016/j.elstat.2016.01.002>

36 Vogel, P. *et al.* Charging of Dielectric Surfaces in Contact with Aqueous Electrolytes—the Influence of CO₂. *Journal of the American Chemical Society* **144**, 21080-21087 (2022). <https://doi.org/10.1021/jacs.2c06793>

37 Petrenko, V. F. & Whitworth, R. W. *Physics of ice*. (OUP Oxford, 1999).

38 Sánchez, M. A. *et al.* Experimental and theoretical evidence for bilayer-by-bilayer surface melting of crystalline ice. *Proceedings of the National Academy of Sciences* **114**, 227-232 (2017). <https://doi.org/10.1073/pnas.1612893114>

39 Bada, J. L., Chalmers, J. H. & Cleaves, H. J. Is formamide a geochemically plausible prebiotic solvent? *Physical Chemistry Chemical Physics* **18**, 20085-20090 (2016). <https://doi.org/10.1039/C6CP03290G>

40 Nie, J. *et al.* Probing Contact-Electrification-Induced Electron and Ion Transfers at a Liquid–Solid Interface. *Advanced Materials* **32**, 1905696 (2020). <https://doi.org/10.1002/adma.201905696>

41 Valtiner, M., Banquy, X., Kristiansen, K., Greene, G. W. & Israelachvili, J. N. The electrochemical surface forces apparatus: the effect of surface roughness, electrostatic surface potentials, and anodic oxide growth on interaction forces, and friction between dissimilar surfaces in aqueous solutions. *Langmuir* **28**, 13080-13093 (2012). <https://doi.org/10.1021/la3018216>

42 Dennis, C. P., Benjamin, A. Y., Aditya, S. K., Paul, J. S. & James, W. S. Formation of charge carriers in liquids. *Advances in Colloid and Interface Science* **244**, 21-35 (2017). <https://doi.org/https://doi.org/10.1016/j.cis.2016.11.004>

43 Di Quarto, F., Sunseri, C., Piazza, S. & Romano, M. C. Semiempirical correlation between optical band gap values of oxides and the difference of electronegativity of the elements. its importance for a quantitative use of photocurrent spectroscopy in corrosion studies. *The Journal of Physical Chemistry B* **101**, 2519-2525 (1997). <https://doi.org/10.1021/jp970046n>

44 Bhandari, U., Ghadimi, H., Zhang, C., Yang, S. & Guo, S. Predicting elastic constants of refractory complex concentrated alloys using machine learning approach. *Materials* **15**, 4997 (2022). <https://doi.org/https://doi.org/10.3390/ma15144997>

45 Leibauer, B. *et al.* How surface and substrate chemistry affect slide electrification. *Journal of the American Chemical Society* **146**, 10073–10083 (2024). <https://doi.org/https://doi.org/10.1021/jacs.4c01015>

46 Leibauer, B. *et al.* Wetting of surface grafted hydrophilic-b-hydrophobic block copolymer brushes. *Advanced Functional Materials* **35**, 2419443 (2025). <https://doi.org/10.1002/adfm.202419443>

47 Keller, R. N., Wrcoff, H. D. & Marchi, L. E. in *Inorganic Syntheses* 1-4 (1946).

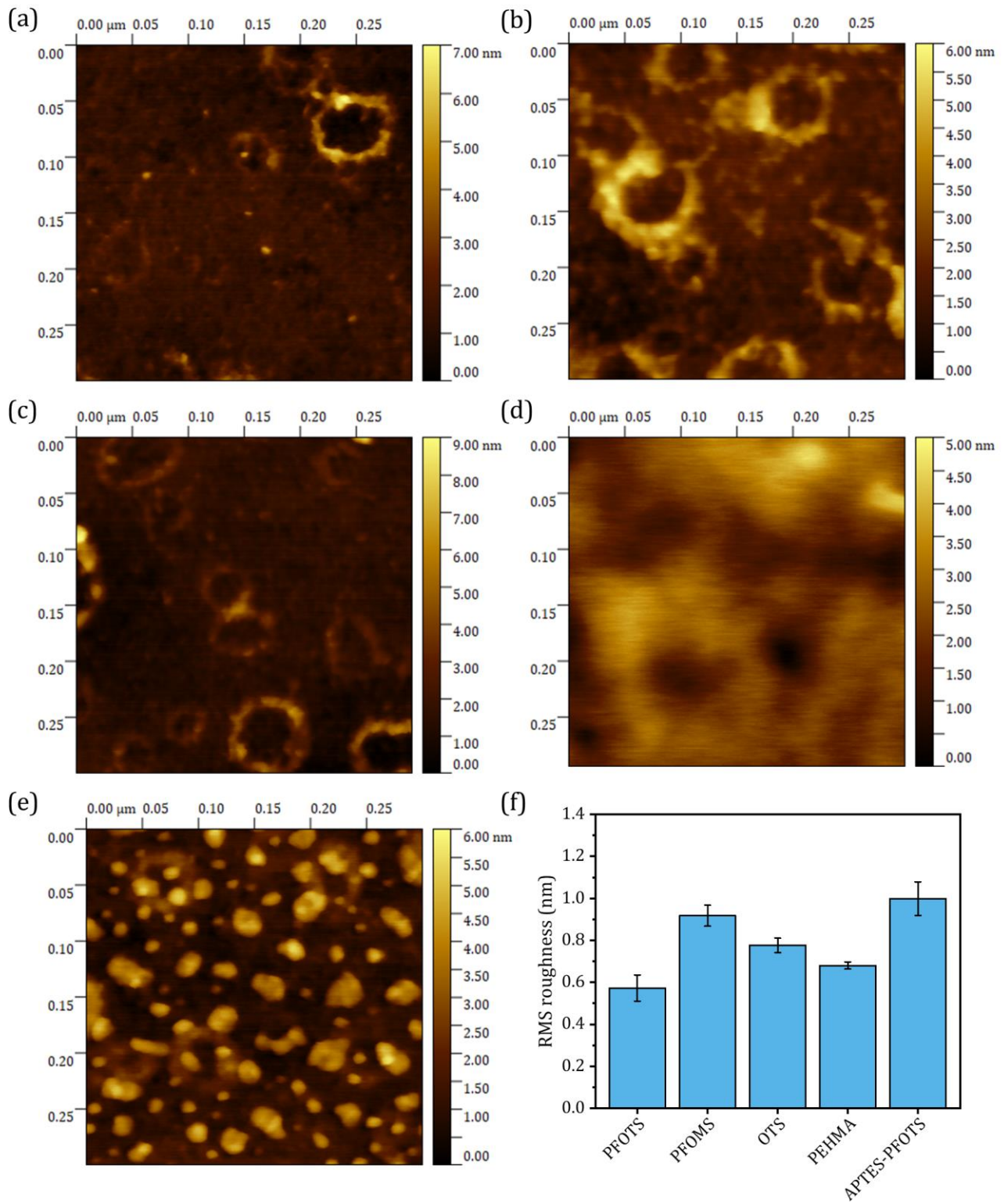
48 Maeda, N. Brief Overview of Ice Nucleation. *Molecules* **26**, 392 (2021). <https://doi.org/https://doi.org/10.3390/molecules26020392>

Two Charging Mechanisms in Contact Electrification of Liquid and Ice

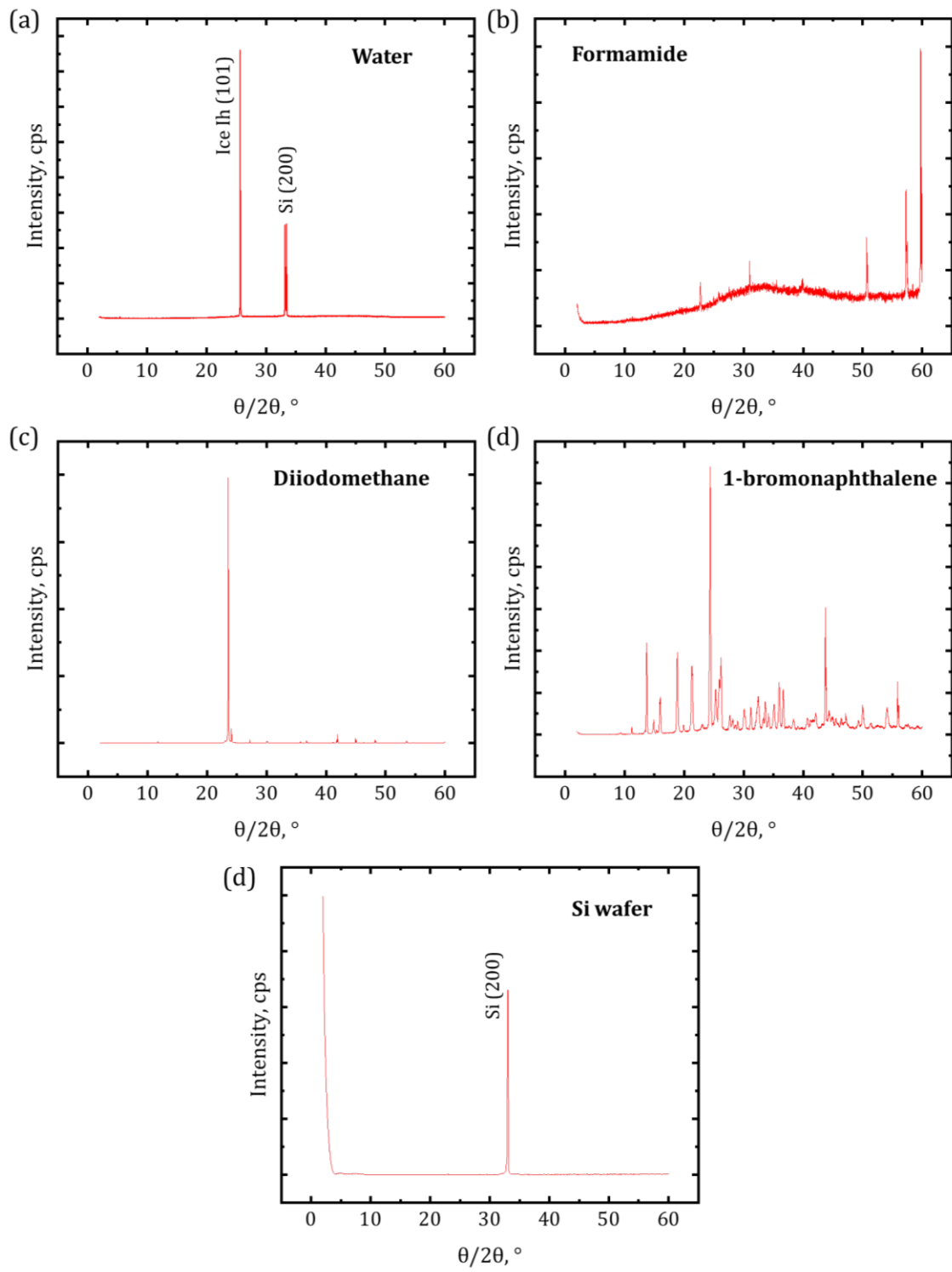
Rutvik Lathia¹; Benjamin Leibauer¹; Aaron D. Ratschow¹; Werner Steffen¹ and Hans-Jürgen Butt^{1,*}

¹ Max Planck Institute for Polymer Research, Ackermannweg 10, 55128 Mainz, Germany

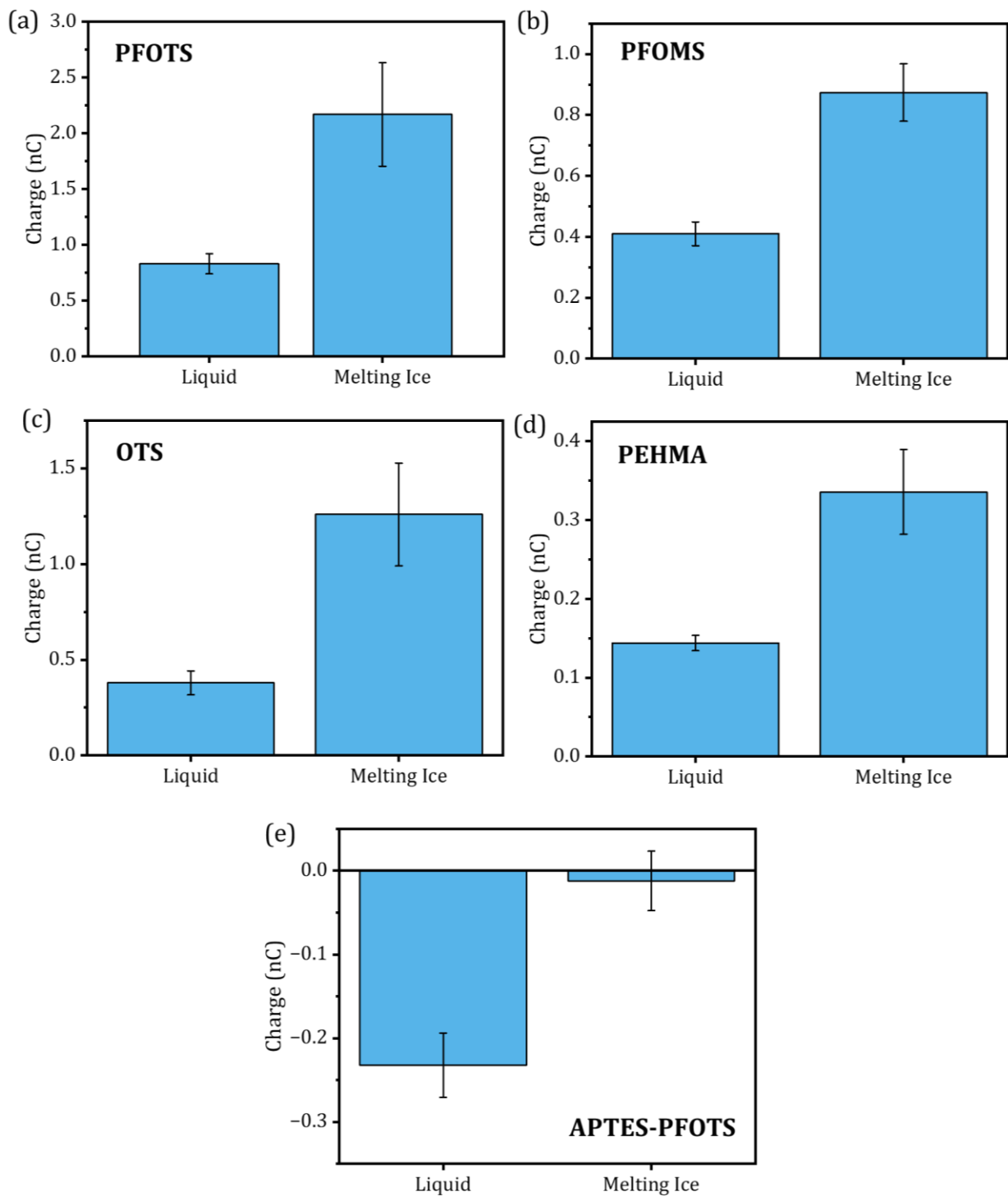
*Corresponding author: butt@mpip-mainz.mpg.de



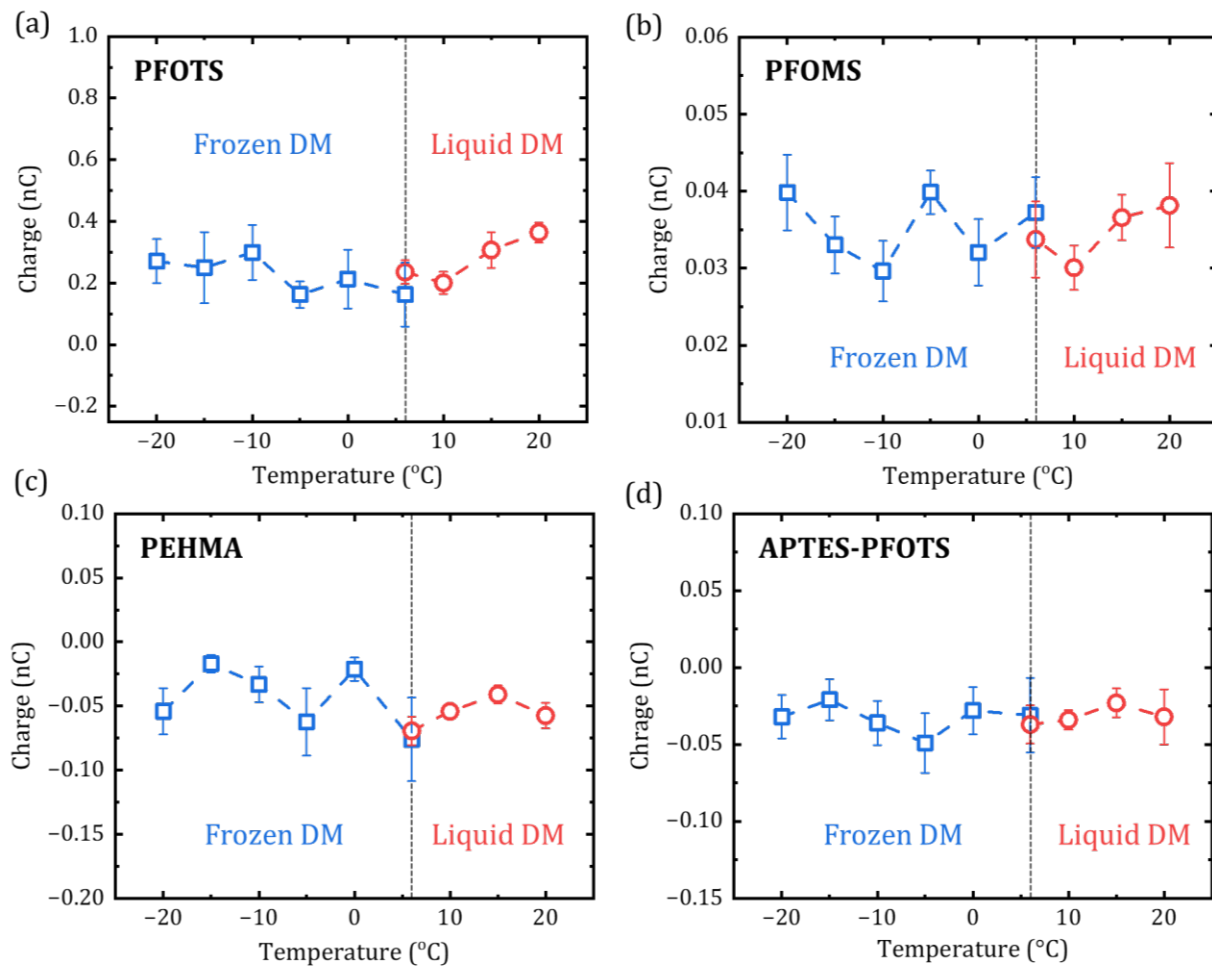
Supplementary Fig. S1: AFM topography images of (a) PFOTS (b) PFOMS (c) OTS (d) PEHMA and (e) APTES-PFOTS on glass. (f) RMS roughness for all the hydrophobic coatings. Error bar represents standard deviation of 3 measurements.



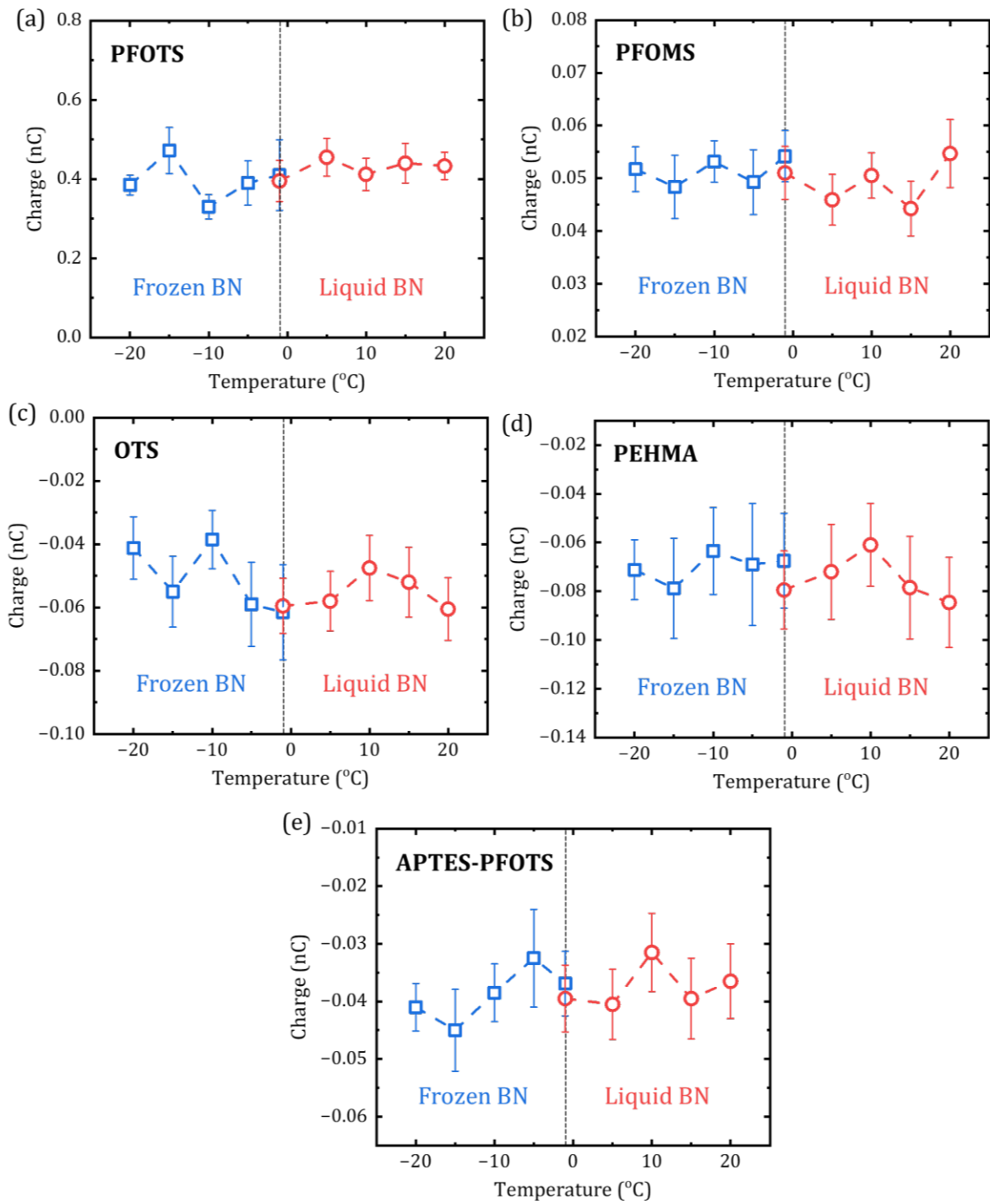
Supplementary Fig. S2: XRD diffractograms for all the frozen chemicals and OTS-coated Si-wafer. Formamide spectra were recorded at -50°C while other all data were acquired at -20°C .



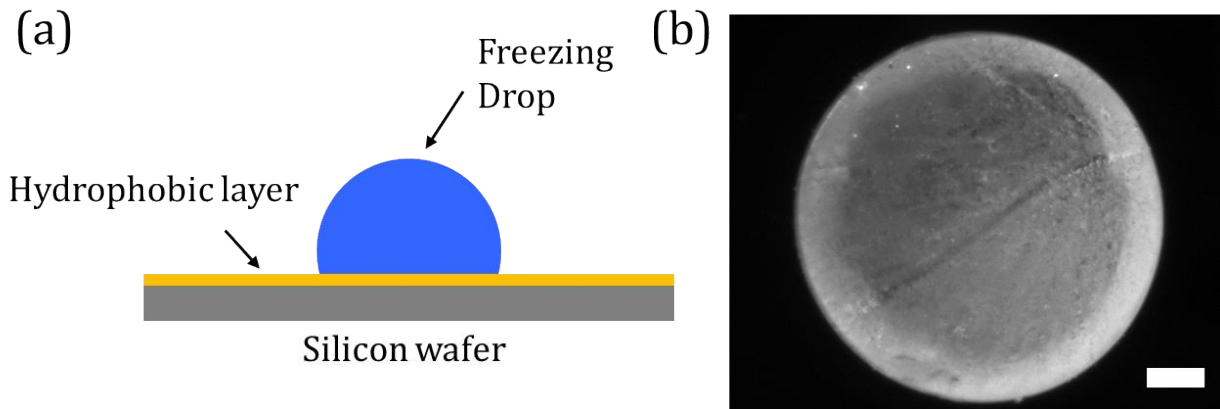
Supplementary Fig. S3: Drop charge of liquid (20 °C) and frozen formamide (-20 °C) measured on the five different surfaces. Formamide was frozen first with liquid nitrogen and then charging measurements were carried out.



Supplementary Fig. S4: Drop charge versus temperature of liquid (red) and frozen (blue) diiodomethane on various surfaces.



Supplementary Fig. S5: Drop charge versus temperature of liquid (red) and frozen (blue) 1-bromonaphthalene on various surfaces.



Supplementary Fig. S6: (a) Droplets deposited on a hydrophobic layer-coated silicon wafer and subsequently frozen. (b) Inverted light microscopy view of the resulting frozen ice (50 μ l) on PFOTS coated silicon wafer. Scale = 1 mm.

Molecule	Average Pauling Electronegativity (χ)
Diiodomethane	2.45
1-bromonaphthalene	2.44
Water	2.61
Formamide	2.61
PFOTS	3.07
OTS	2.37
PFOMS	2.98
PEHMA	2.38

Table S1: Average Pauling electronegativity (χ) of various molecules used for calculating Δ_{en} .